Necking Behavior in High-Speed Melt Spinning of Poly(ethylene terephthalate)

JUNG SUN KIM, SANG YONG KIM

Department of Fiber and Polymer Science, College of Engineering, Seoul National University, San 56-1, Shinlim-Dong, Kwanak-Ku, Seoul 151-742, Korea

Received 22 March 1999; accepted 20 April 1999

ABSTRACT: The necking behavior in the high-speed melt-spinning process of poly(ethylene terephthalate) (PET) was analyzed using a mathematical simulation under a nonisothermal condition. A constitutive model into which the strain-rate dependence of viscosity and the strain-hardening effect are incorporated was used. Based on the simulated results, the cause of a local reduction of apparent viscosity was found to be due mainly to high strain rate. Also the onset of crystallization, if it occurred, was found to happen near the end of the neck. In addition, with no crystallization involved, the necking can still occur. The deformation process in high-speed spinning of PET was found to consist of two regions along the spin line: a Newtonian flow region and a rubberlike deformation region. The necking behavior is discussed here in terms of strain-rate sensitivity and strain-hardening parameter. As a result, a criterion for the onset of stable necking has been obtained. The necking behavior does not seem to be essentially different from that in cold drawing. © 2000 John Wiley & Sons, Inc. J Appl Polym Sci 76: 446–456, 2000

Key words: necking; high-speed spinning; poly(ethylene terephthalate); strain-rate sensitivity; strain hardening

INTRODUCTION

It is well known that the high-speed melt spinning of crystallizing polymers is generally accompanied by abrupt diameter attenuation right above the solidification point in the spin line. This behavior is so similar to the necking phenomenon frequently observed in cold drawing that such a deformation in high-speed melt spinning is referred to as a "necklike deformation." The control of the necking behavior leads to enhanced structure and properties of high-speed spun fibers because the major structure development in fibers takes place within the necking zone in the spin line.

Kase[1] suggested that the cold-drawing theory is valid in the necklike deformation in high-speed melt spinning and that the necking phenomenon is due to the constitutive nature of the polymer. Many efforts have also been made to account for the necking phenomenon in high-speed melt spinning. In earlier approaches the necking mechanism in high-speed melt spinning has been discussed in terms of rheological and dynamic factors.[2] The effect of crystallization on necklike deformation has also been considered.[3,4] In order to produce a necklike deformation by use of these models, a local reduction of viscosity due to the released heat of crystallization was required. However, it was shown by a semiempirical method that the reduction of viscosity appears when a necklike deformation occurs, although the filament temperature decreases monotonically without any peak or plateau along the spin line.[5,6]

Correspondence to: J. S. Kim (kjsphj@crosswinds.net).

Journal of Applied Polymer Science, Vol. 76, 446–456 (2000)
© 2000 John Wiley & Sons, Inc.

This suggests that the local reduction of viscosity may be attributed to the high strain rate when the necklike deformation occurs. This idea is supported by the well-known fact that elongational viscosity tends to decrease at high strain rates.[7]

The necking behavior has also been discussed in terms of high Deborah number viscoelastic responses coupled with nonisothermal conditions.[8] In addition to this approach, it was proposed that axial and radial viscosity variations could cause the necklike deformation in high-speed melt spinning.[9,10] There has been an attempt to treat the necklike deformation in high-speed melt spinning as a problem of sensitivity to external disturbances.[11]

Recently, a qualitative one-dimensional isothermal model was proposed on the basis of the interaction between the internal microstructure development and flow deformation.[12] According to this model, the structural changes caused by the onset of crystallization can result in neck formation. Therefore, this model is based on the assumption that the onset of crystallization triggers necklike deformation.

Mathematical simulations have been carried out to describe the necking phenomenon using simple nonisothermal models.[13–16] Due to lack of information, several arbitrary assumptions were made for these calculations. The effect of orientation-induced crystallization has been incorporated in some models.[13,14] However, those mathematical simulations failed to describe necklike deformation without arbitrary assumptions.

In this article the necking phenomenon in high-speed spinning is considered to originate from a constitutive nature of the polymer. According to Haberkorn et al.,[6] it was concluded with a good degree of approximation that the necking is caused by a rubber–elastic deformation of the melt. This suggests that the effect of strain hardening due to molecular orientation is too significant to be neglected. In addition to this, the strain-rate dependence of viscosity is considered another crucial factor. Therefore, in order to elucidate the necking behavior in the high-speed spinning process of poly(ethylene terephthalate) (PET), we have adopted a more refined constitutive relation that takes into account not only the strain-rate dependence of viscosity but also strain hardening, and we carried out a mathematical simulation under a nonisothermal condition.

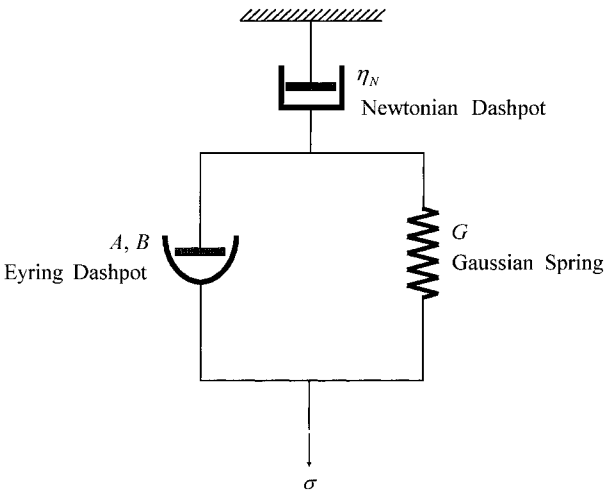

Figure 1 Schematic diagram of the constitutive model adopted in this study.

EXPERIMENTAL

Constitutive Relation

In Figure 1, a one-dimensional constitutive model is represented schematically. As is evident, a Newtonian unit and a Gauss–Eyring unit[17] are connected in series. Due to the series connection of two units, the total true strain rate, $\dot{\varepsilon}$, is the sum of two contributions, that is

$$\dot{\varepsilon} = \frac{\sigma}{\eta_N} + \dot{\varepsilon}_E \tag{1}$$

where σ is a stress applied to the system, η_N is the Newtonian viscosity, and $\dot{\varepsilon}_E$ is a strain-rate contribution of the second unit, which is expressed according to the Gauss–Eyring model as follows

$$\dot{\varepsilon}_E = A\sinh[B(\sigma - \sigma_R)] \tag{2}$$

A and B are functions of temperature that obey the Eyring viscosity law,[18] and σ_R is a rubberlike internal stress[19] represented as:

$$\sigma_R = G\left(\lambda_E^2 - \frac{1}{\lambda_E}\right) \tag{3}$$

where G is the modulus of the Gaussian spring and λ_E is the deformation ratio of the Gauss–Eyring unit.

In this constitutive model, for simplicity, the Gaussian concept is used to account for the strain-hardening behavior instead of a Langevin

concept,[19] since both concepts have the same origin. Because the rubber elastic stress has an entropic origin, deformation will be hardened if available conformations are almost consumed in the material. In this context, it is σ_R that is attributed to the development of molecular orientation.

Mathematical Simulation

The description of the nonisothermal high-speed spinning process at a steady state requires three balance equations—of mass, momentum, and energy—and a constitutive relation.

1. Mass balance:

$$W = \rho \frac{\pi D^2}{4} V \tag{4}$$

2. Momentum balance:

$$\frac{dF}{dz} = W\left(\frac{dV}{dz} - \frac{g}{V}\right) + \frac{\pi}{2} \rho_a C_f V^2 \tag{5}$$

3. Energy balance:

$$\frac{dT}{dz} = -\frac{\pi D h}{W C_p} (T - T_a) + \frac{\Delta H}{C_p} \frac{dX_c}{dz} \tag{6}$$

4. Constitutive equation:

$$\frac{dV}{dz} = \frac{\sigma}{\eta_N} + A \sinh\left[B\left\{\sigma - G\left(\lambda_E^2 - \frac{1}{\lambda_E}\right)\right\}\right] \tag{7}$$

where D, V, F, T, and X_c are filament diameter, axial velocity, spin-line tension, filament temperature, and crystallinity, respectively, at a distance z from the spinneret; ρ, C_p, and ΔH are density, specific heat, and heat of fusion, respectively, of the polymer; C_f and h are air drag coefficient and convective coefficient, respectively, of heat transfer; W is mass flow rate; g is acceleration of gravity; ρ_a and T_a are air density and cooling air temperature, respectively; and $\sigma = 4F/\pi D^2$ is the tensile stress. More details are given elsewhere.[13]

In the mathematical model used in this study, the orientation-induced crystallization is also taken into account. Nakamura et al.[20] proposed a modified Avrami equation by defining the relative crystallinity, $\theta = X_c/X_\infty$, as

$$\theta = 1 - \exp\left[-\left(\int_0^t K\, dt\right)^n\right] \tag{8}$$

where X_∞ is the limiting crystallinity and K is the crystallization-rate constant that is a function of temperature and orientation parameter, such as birefringence. For the crystallization-rate constant in this study, the following expression for PET proposed by Katayama and Yoon[15] is adopted

$$\frac{K}{K_0} = \exp\left[\frac{1.2 \times 10^6}{(T + 273)\Delta T} \times \left\{1 - \frac{1}{1 + 160(T + 273)(\Delta n)^2/\Delta T}\right\}\right] \tag{9}$$

where K_0 denotes the crystallization-rate constant dependent only on temperature:

$$K_0 = \exp\left[9.34 - \frac{682}{T - 43} - \frac{4.53 \times 10^5}{(T + 273)\Delta T}\right] \tag{10}$$

On the ground that Δn is, in general, related to $\sigma/(T + 273)$ according to the theory of rubber elasticity, Katayama and Yoon[15] also postulated the following relation for PET.

$$\Delta n = 0.2\left[1 - \exp\left\{-\frac{1.65 \times 10^{-6}\sigma}{T + 273}\right\}\right] \tag{11}$$

In the present model, however, only the rubberlike internal stress is assumed to contribute to the development of orientation, and thus Eq. (11) is modified as follows:

$$\Delta n = 0.2\left[1 - \exp\left\{-\frac{1.65 \times 10^{-6}\sigma_R}{T + 273}\right\}\right] \tag{12}$$

Because crystallization takes place in the spin line in high-speed melt spinning, material parameters are functions not only of temperature but also of crystallinity. Therefore, the crystallization effect should be incorporated in the material parameters. In order to represent its contribution to the material parameters, exponential factors are used in the present model. As a result, the material parameters used in this simulation are assumed to have the following forms

$$G = a_1 \exp\left(\frac{a_2}{T + 273}\right) \exp(6\theta^2) \tag{13}$$

$$\eta_N = a_3 \exp\left(\frac{a_4}{T + 273}\right) \exp(12\theta^2) \tag{14}$$

$$A = a_5 \exp\left(-\frac{a_6}{T + 273}\right)\exp(-12\theta^2) \quad (15)$$

$$B = \frac{a_7}{T + 273} \quad (16)$$

where a_1, a_2, a_3, a_4, a_5, a_6, and a_7 are constants. Because there are no available experimental data for these constants, the most plausible set of constants has been taken from arbitrary sets. The values of constants obtained in this method are as follows: $a_1 = 0.45 \times 10^{-3}\ CF$, $a_2 = 0.512 \times 10^4$, $a_3 = 0.413$, $a_4 = 0.695 \times 10^4$, $a_5 = 4.81 \times 10^{10}$, $a_6 = 0.938 \times 10^4$, and $a_7 = 7.41 \times 10^{-5}$. In particular, CF in a_1 is used as a correction factor to express the effect of the average deformation rate on the modulus:

$$CF = 1 + d_1\left(\frac{V_L}{L}\right)^{d_2} \quad (17)$$

where V_L and L are the spinning speed and the spinning distance, respectively; $d_1 = 1.376 \times 10^{-6}$ and $d_2 = 4.5$. With this set of constants and the above-mentioned relations, the calculation of the model gives a satisfactory result.

RESULTS AND DISCUSSION

The melt-spinning process of PET was simulated for two mass flow rates under free convection at the spinning temperature of 290°C. The assumed spinneret diameter and spinning distance were 500 μm and 330 cm, respectively.

The calculated diameter and temperature profiles are shown in Figures 2 and 3, respectively. As is evident from Figure 2, the necklike deformation is observed at higher spinning speeds above 3000 m/min, and the intensity of the neck also increases with increasing spinning speed. In addition, as the spinning speed increases, the solidification point moves upstream along the spin line. At the same spinning speed, the solidification point in the case of the low mass flow rate is located farther away from the spinneret than in the case of high mass flow rate. This suggests that the draw-down ratio controls the position of the solidification point. The solidification temperature also increases with increasing spinning speed.

As can be seen in Figure 3, the spinning speed, as in general, has only a minor effect on the temperature profiles. However, this is not the case when the crystallization takes place in the spin line. In this case, the heat of crystallization is released, and thus the filament temperature tends to increase, which is followed by the appearance of a plateau or even a peak in the temperature profile. It is observed in Figure 4 that, at 7000 m/min, the significant crystallization takes place in the spin line. As a result of the heat of crystallization, a peak indeed appears in the temperature profile calculated at 7000 m/min. As will

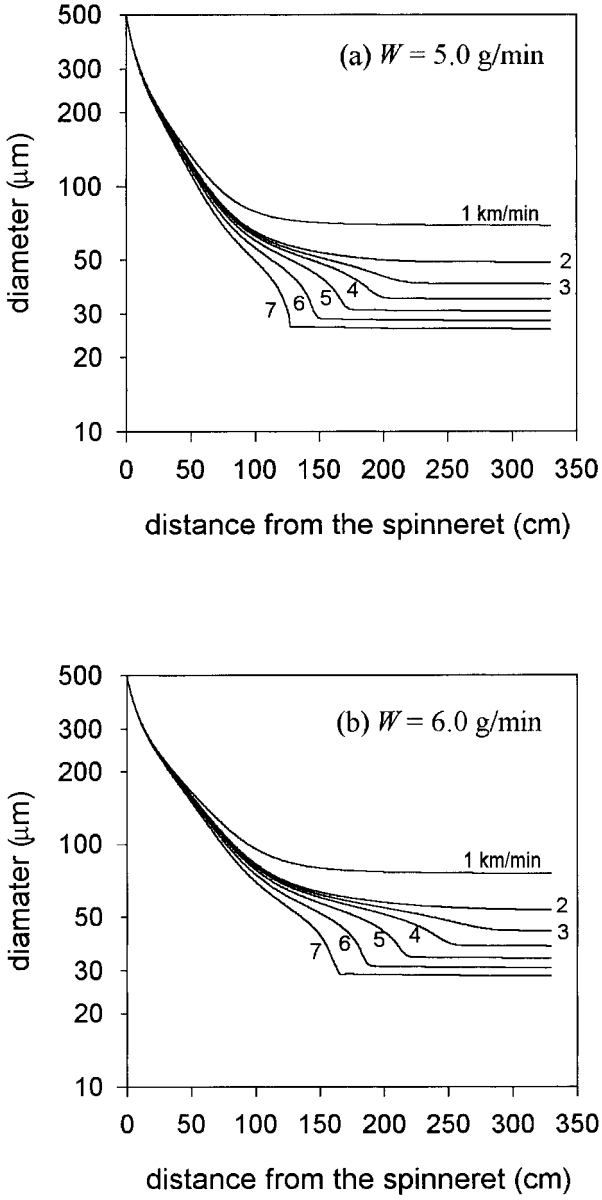

Figure 2 Calculated diameter profiles for mass flow rates of (a) 5.0 g/min and (b) 6.0 g/min. The spinning speed (km/min) for each case is indicated.

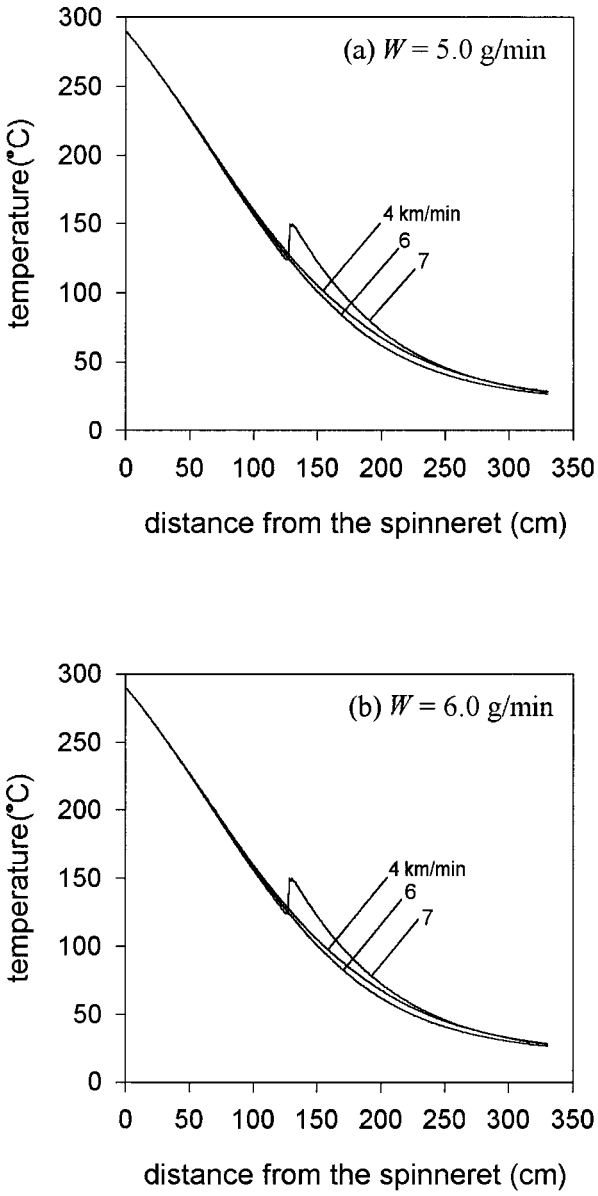

Figure 3 Calculated temperature profiles for mass flow rates of (a) 5.0 g/min and (b) 6.0 g/min. The spinning speed (km/min) for each case is indicated.

be demonstrated later, the temperature rise does not affect the necking behavior.

Figure 5 shows the calculated stress profiles. The steady increase of stress even below the solidification point is attributed to the air drag effect, which is significant in the high-speed melt-spinning process. The stress has a little higher value in the case of the low mass flow rate than in the case of the high mass flow rate. This is because a lower mass flow rate produces a higher draw-down ratio under the condition of the same spinning speed. It is interesting to note that the positive curvature is observed right above the solidification point in the stress profiles calculated at spinning speeds that produce necklike deformation. It is taken for granted that this is due mainly to the abrupt decrease of the cross-sectional area when the necklike deformation occurs.

Figure 6 shows the calculated birefringence profiles. Because the birefringence can be used as

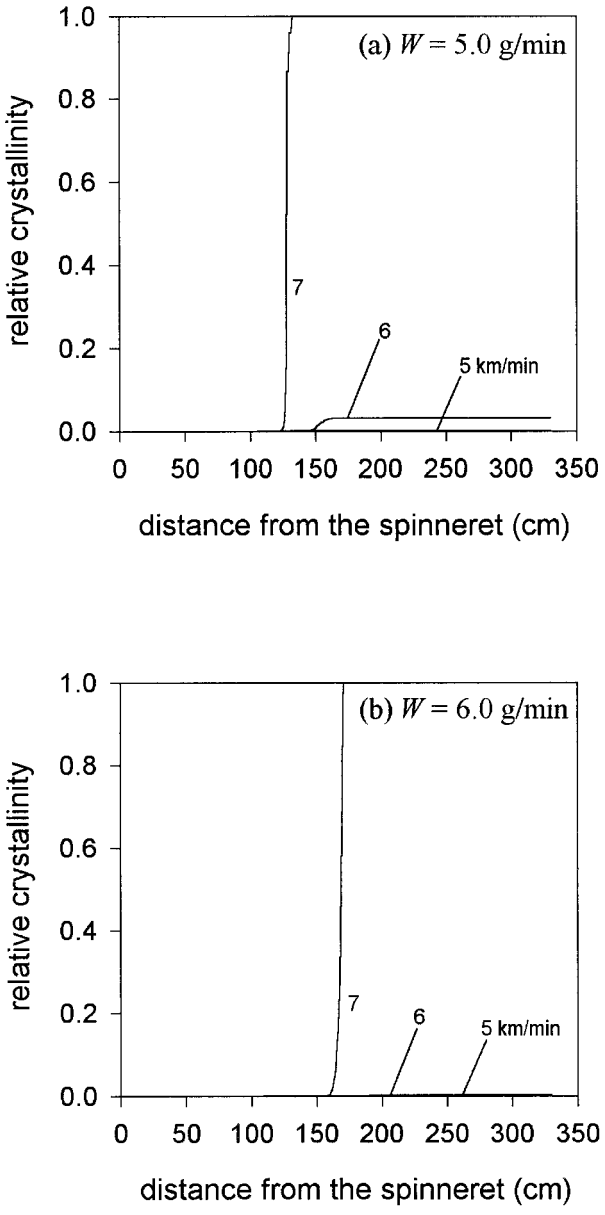

Figure 4 Calculated relative crystallinity profiles for mass flow rates of (a) 5.0 g/min and (b) 6.0 g/min. The spinning speed (km/min) for each case is indicated.

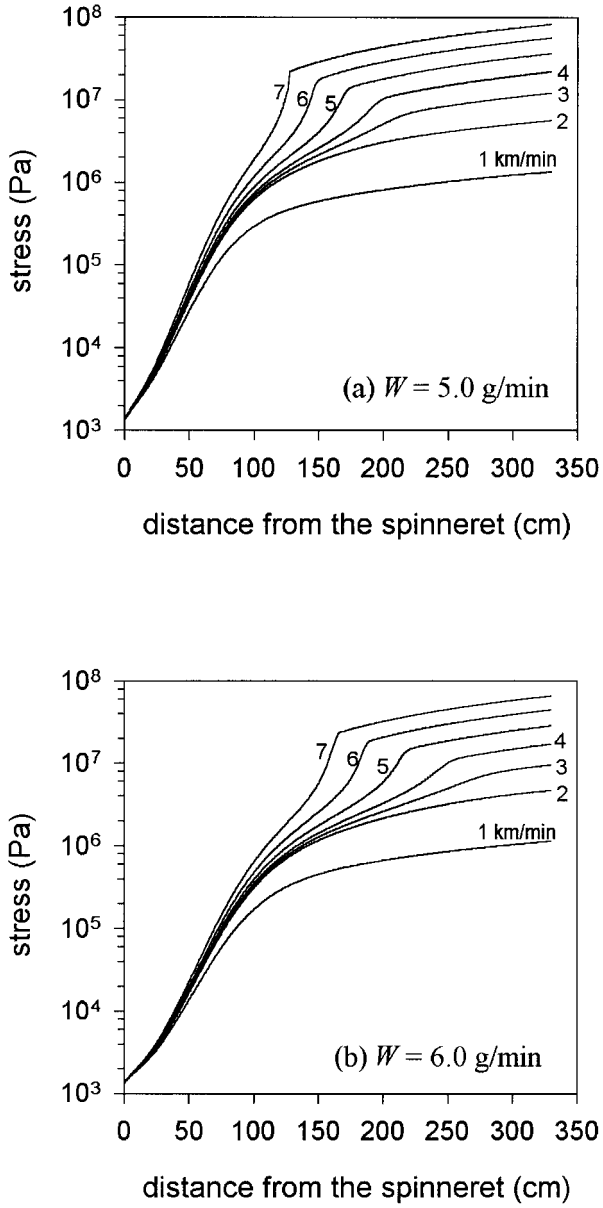

Figure 5 Calculated stress profiles for mass flow rates of (a) 5.0 g/min and (b) 6.0 g/min. The spinning speed (km/min) for each case is indicated.

a measure of orientation developed in the material and the orientation is assumed to be controlled only by the rubberlike internal stress, the degree of strain hardening can also be predicted by the birefringence. As expected, the final birefringence and its increasing rate increase as the spinning speed increases. It follows that the higher spinning speed results in a more significant strain hardening because of the resulting higher draw-down ratio, which is closely related to the necking behavior.

Figure 7 shows the calculated strain-rate profiles. At spinning speeds above 3000 m/min, with increasing spinning speed, the maximum strain rate increases; furthermore, its position shifts toward the spinneret along the spin line. On the contrary, in the case of lower spinning speeds, the position of the maximum strain rate shifts toward the take-up device with increasing spinning speed. This is a typical trend of Newtonian fluids. It can be concluded from this and from the birefringence behavior that the deformation process

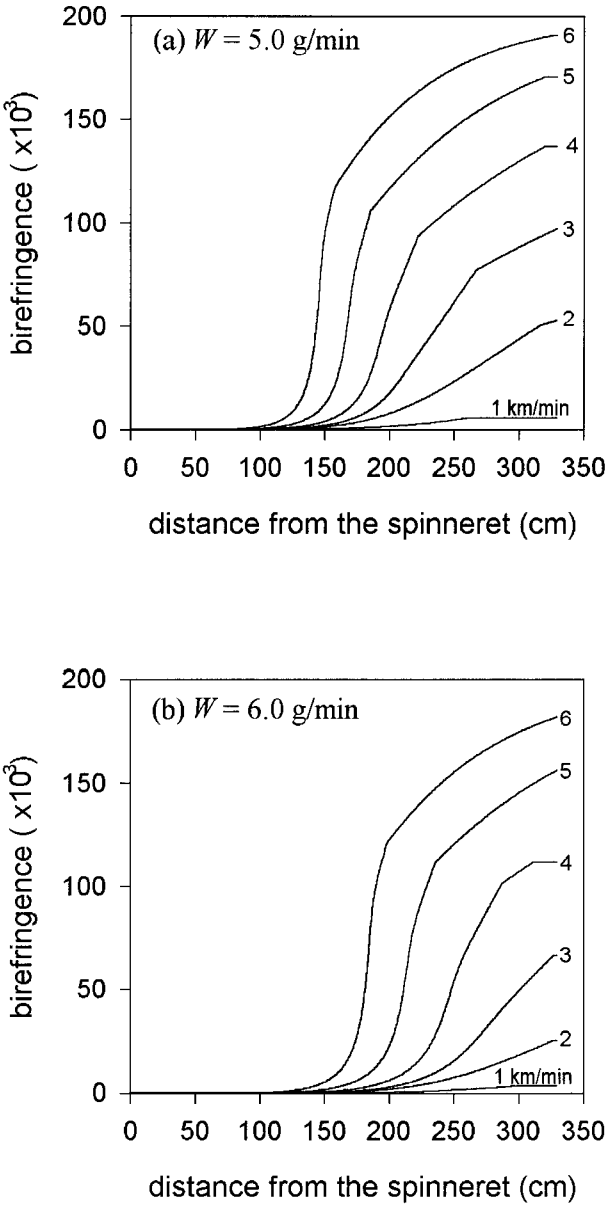

Figure 6 Calculated birefringence profiles for mass flow rates of (a) 5.0 g/min and (b) 6.0 g/min. The spinning speed (km/min) for each case is indicated.

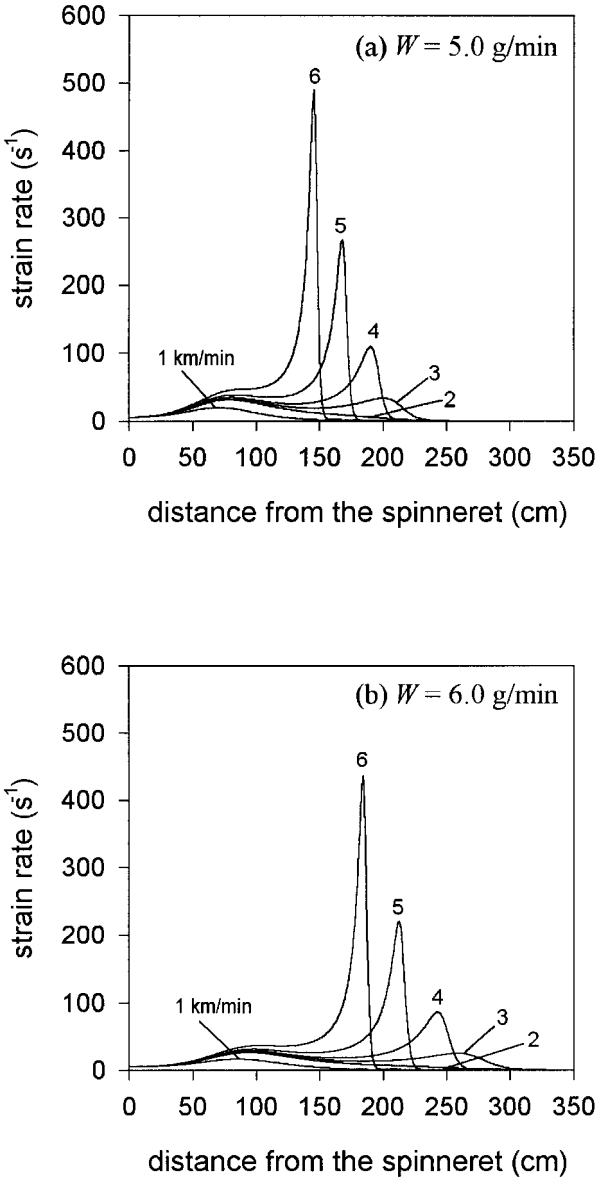

Figure 7 Calculated strain-rate profiles for mass flow rates of (a) 5.0 g/min and (b) 6.0 g/min. The spinning speed (km/min) for each case is indicated.

in high-speed melt spinning consists of two regions: one is a nonorientational flow region and the other an orientational deformation region equivalent to the rubberlike deformation region. Most deformation in lower-speed spinning takes place in the former region, so that the final birefringence is very low. On the contrary, most of the deformation in higher-speed spinning tends to be concentrated in the latter region, so that the final birefringence is much higher.

It is evident from Figures 2 and 8 that the formation of the neck is closely associated with the local reduction of apparent viscosity. As the spinning speed increases, the viscosity reduction becomes more localized and sharper, and simultaneously the intensity of the neck becomes higher. It is certain that the necklike deformation does not occur without the local reduction of viscosity. It is easy to show that the local reduction of viscosity is nearly independent of the temperature rise due to the exothermic effect of crystallization. This is evident from Figure 9, where the calculated profiles of diameter, temperature, ap-

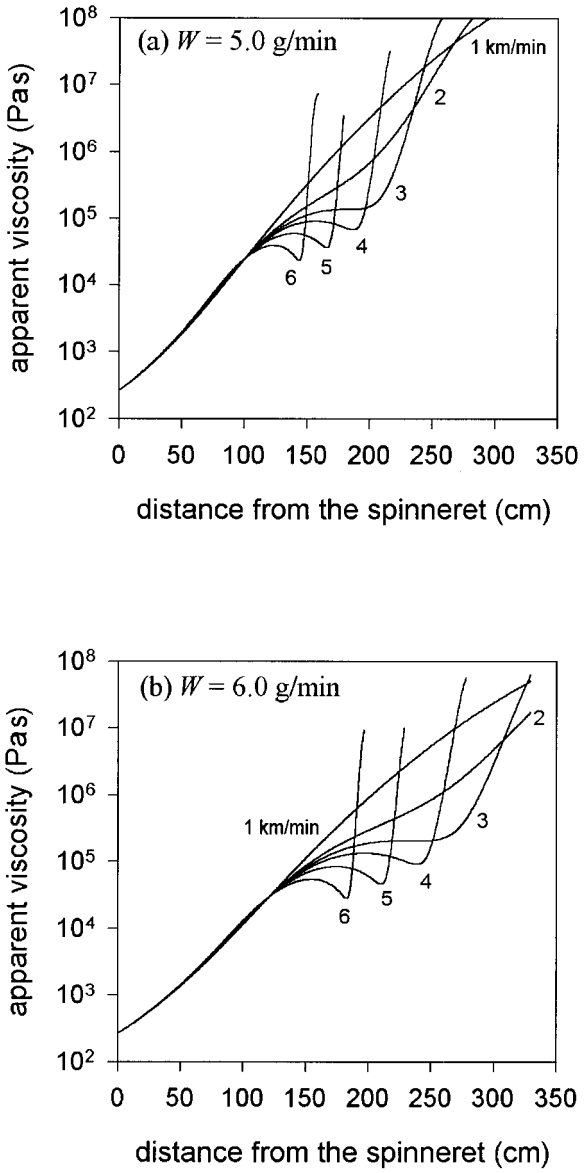

Figure 8 Calculated apparent viscosity profiles for mass flow rates of (a) 5.0 g/min and (b) 6.0 g/min. The spinning speed (km/min) for each case is indicated.

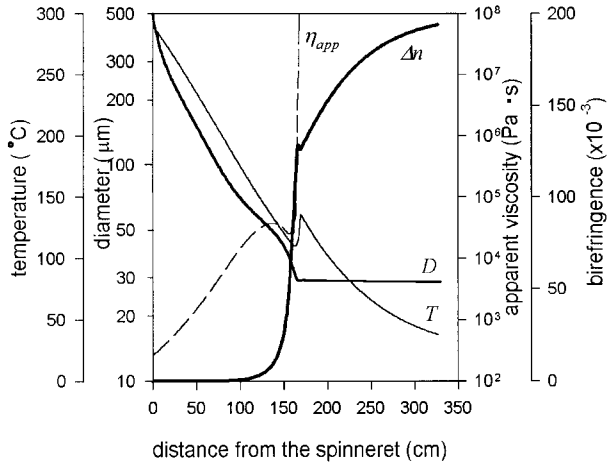

Figure 9 Calculated profiles of diameter (D), temperature (T), apparent viscosity (η_{app}), and birefringence (Δn) for a mass flow rate of 6.0 g/min and a spinning speed of 7000 m/min.

parent viscosity, and birefringence for 6.0 g/min and 7000 m/min are shown. Generally speaking, the effect of crystallization on the viscosity is dual: although the temperature rise due to the heat of crystallization causes the apparent viscosity to decrease, the solidification is accelerated by the onset of crystallization, followed by an increase in the apparent viscosity. Judging from the above results, the latter effect turns out to be much more dominant.

From Figures 2 through 10, it can be seen that the following mechanism is possible: As the strain rate increases along the spin line, the apparent viscosity approaches the maximum at the point where the onset of necking takes place. As the filament cross section decreases suddenly due to the formation of the neck, the stress increases steeply, during which the strain rate passes its maximum at the point where the viscosity approaches its minimum. The degree of orientation increases significantly because of a very high internal stress, so the number of available conformations for the polymer chains decreases rapidly and hence a strain hardening occurs. As the strain hardening progresses, the necklike deformation comes to its end. At the latter part of the neck, the onset of orientation-induced crystallization occurs, during which the heat of crystallization manifests itself in the spin line as a peak in the temperature profile. Finally, the filament is solidified and the deformation process stops.

Based on results from the present model, it appears that although no crystallization occurs in the spin line, the necklike deformation can take place. This indicates that the onset of necking is hardly associated with the kinetics of orientation-induced crystallization. Instead, the local reduction of apparent viscosity due to the high strain rate and the deformation hardening may be the essential factors in controlling the necking behavior. It is certain from Figures 9 and 10 that the former is attributed not to the temperature rise caused by the heat of crystallization but to the high strain rate.[7] On the other hand, the latter is affected mainly by the draw-down ratio, and because of this, the necklike deformation is hardly

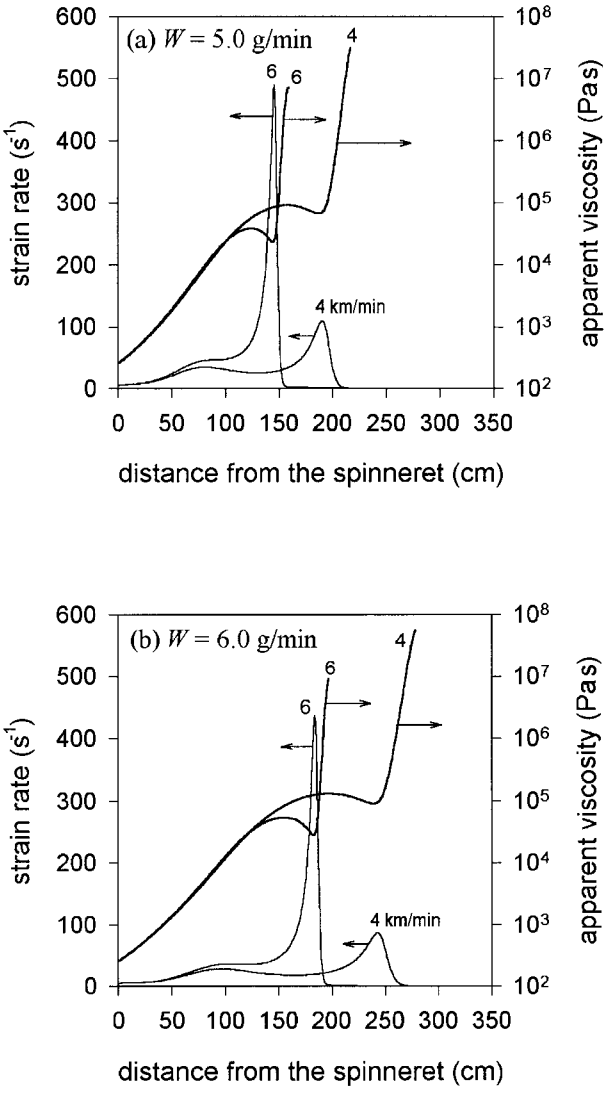

Figure 10 Comparison of behaviors of strain rate and apparent viscosity for mass flow rates of (a) 5.0 g/min and (b) 6.0 g/min. The spinning speed (km/min) for each case is indicated.

expected to occur in the spinning at lower speeds and higher flow rates.

The strain-hardening parameter and strain-rate sensitivity,[21,22] which are well known in cold drawing, are introduced to analyze the necking behavior in the present study. It is preferable to define their dimensionless forms as follows:

$$\gamma = \frac{1}{\sigma}\left(\frac{\partial \sigma}{\partial \varepsilon}\right)_{\dot{\varepsilon}} \tag{18}$$

$$m = \frac{\dot{\varepsilon}}{\sigma}\left(\frac{\partial \sigma}{\partial \dot{\varepsilon}}\right)_{\varepsilon} \tag{19}$$

where γ and m are the strain-hardening parameter and strain-rate sensitivity, respectively, and ε is the true strain. When $\gamma = 1$, the Considère construction is satisfied, and thus a neck propagates in a stable manner. In this sense, γ defines the stability of the neck. On the contrary, m is known to control the intensity of the neck. A smaller value of m produces a sharper neck.

Now consider two limiting cases. For generalized Newtonian fluids, $\sigma = \eta(\dot{\varepsilon})\ \dot{\varepsilon}$, there is no strain hardening since stress is independent of strain, while the strain-rate sensitivity, m, is derived as follows:

$$m = \frac{\dot{\varepsilon}}{\sigma}\left(\frac{\partial \sigma}{\partial \dot{\varepsilon}}\right)_{\varepsilon} = 1 + \frac{d \ln \eta(\dot{\varepsilon})}{d \ln \dot{\varepsilon}} \tag{20}$$

From this equation the conclusion can be drawn that it's always true $m \leq 1$ because the viscosity is generally a decreasing function of the strain rate. The equality, that is, $m = 1$, is satisfied in the case of the Newtonian limit. Therefore, on the basis of the above concept, the Newtonian fluids show no necking phenomena at all, and even for the generalized Newtonian fluids, the necking can hardly occur because there's no strain-hardening effect. Rubberlike solids assuming a Gaussian network can be taken as another limit, expressed as $\sigma = G(\lambda^2 - 1/\lambda)$, where λ is the deformation ratio and thus $\varepsilon = \ln \lambda$. At a glance, it can be seen that there is no strain-rate sensitivity, that is, $m = 0$, and the strain-hardening parameter is derived as follows:

$$\gamma = \frac{\lambda}{\sigma}\left(\frac{\partial \sigma}{\partial \lambda}\right)_{\dot{\varepsilon}} = \frac{2\lambda^3 + 1}{\lambda^3 - 1} \tag{21}$$

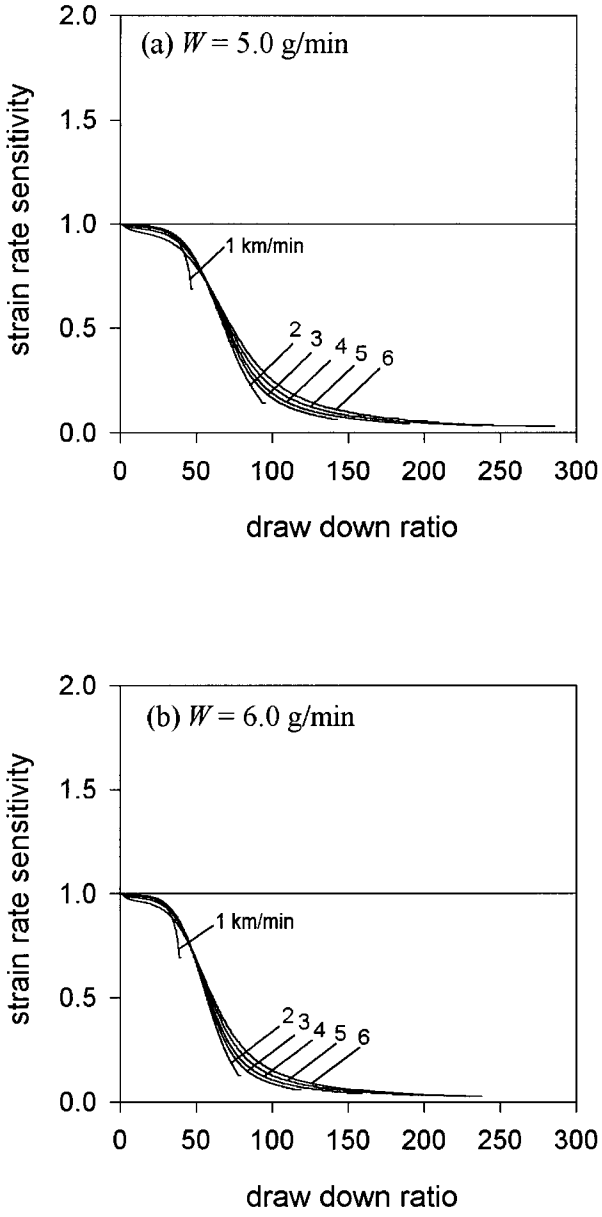

Figure 11 Strain-rate sensitivity for mass flow rates of (a) 5.0 g/min and (b) 6.0 g/min. The spinning speed (km/min) for each case is indicated.

In this case, γ is evidently always >1, so that the strain-hardening effect is too significant for the necking to occur.

Following the definitions of γ and m, each parameter was easily calculated and plotted in Figures 11 and 12, respectively. As demonstrated from these figures, there exists a Newtonian region where $m \approx 1$ and $\gamma \approx 0$ at lower draw-down ratios. This is equivalent to the former region in the deformation process along the spin line, which

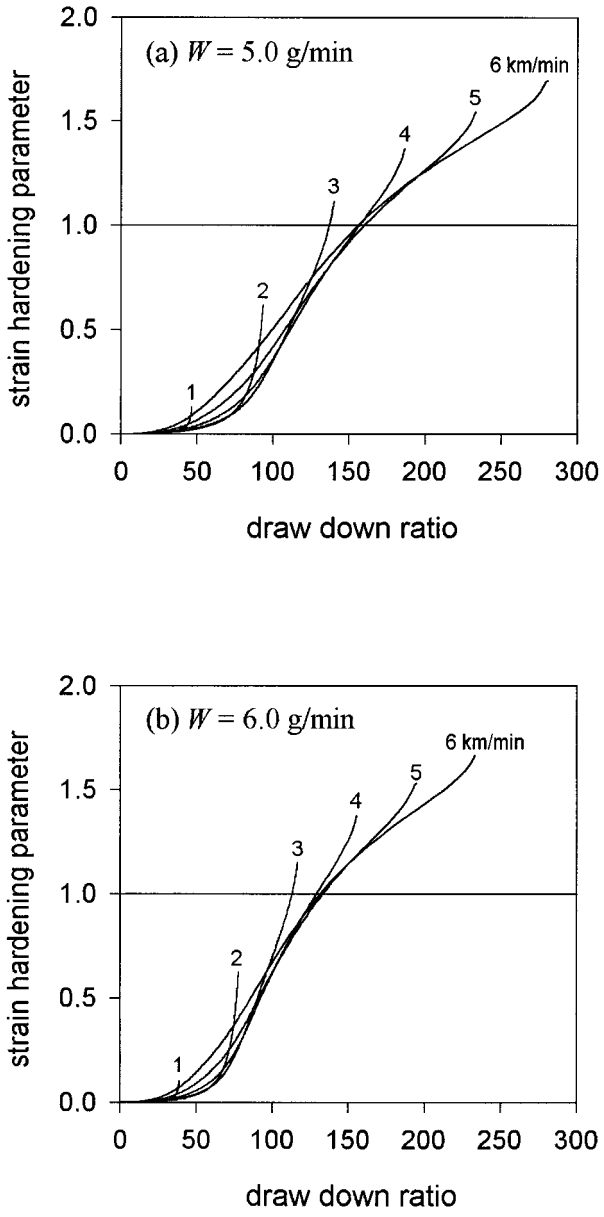

Figure 12 Strain-hardening parameters for mass flow rates of (a) 5.0 g/min and (b) 6.0 g/min. The spinning speed (km/min) for each case is indicated.

has already been mentioned, suggesting that a Newtonian constitutive model is sufficient to describe the conventional low-speed melt-spinning process. With an increasing draw-down ratio, the strain-rate sensitivity decreases while the strain-hardening parameter increases, meaning that the polymer concerned behaves like a rubber at higher draw-down ratios. It should be noted that, for a given mass flow rate, each point where the condition of $\gamma = 1$ is satisfied coincides at nearly the same point, regardless of the spinning speed. This indicates that, in order for the onset of stable necking to occur, the spinning speed should be beyond a particular value for a given mass flow rate.

CONCLUSIONS

In order to analyze the necking behavior in high-speed melt spinning of PET, a mathematical simulation has been carried out, using the nonlinear constitutive relation into which both strain-rate dependence of viscosity and strain hardening have been incorporated. The necking phenomenon has been successfully produced with no arbitrary solidification points imposed.

According to this model, the local reduction of apparent viscosity is caused mainly by the high strain rate due to the abrupt diameter attenuation within the necking zone. In contrast, the effect of the heat of crystallization on the apparent viscosity is relatively negligible. Furthermore, the necking phenomenon can occur even without crystallization. Even if significant crystallization occurs, it starts near the end of the neck.

The deformation process in the high-speed melt spinning of PET has proved to consist of two regions along the spin line: a Newtonian flow region and a rubberlike deformation region. In the latter region, not only does the strain rate increase steeply, but significant strain hardening also takes place and thus the necking can appear. Consequently, in order to describe the necking phenomenon in the high-speed melt spinning of PET, the constitutive relation has to include the strain-rate dependence of viscosity and the strain-hardening effect as well.

The calculated data of the dimensionless strain-hardening parameter and strain-rate sensitivity have shown that the onset of stable necking requires that there exist a point where $\gamma = 1$ in the spin line. In this context, it may be concluded that the necking behavior in the high-speed melt spinning of PET is not essentially different from that in cold drawing.

REFERENCES

1. Kase, S. In High-Speed Fiber Spinning; Ziabicki, A.; Kawai, H., Eds.; Wiley-Interscience: New York, 1985.
2. Ziabicki, A. J Non-Newtonian Fluid Mech 1988, 30, 141.

3. Ziabicki, A. J Non-Newtonian Fluid Mech 1988, 30, 157.
4. Ziabicki, A. Fundamental of Fiber Formation; Wiley: London, 1976.
5. Fujimoto, K.; Iohara, K.; Owaki, S.; Murase, Y. Sen-I Gakkaish 1988, 44, 53.
6. Haberkorn, H.; Hahn, K.; Breuer, H.; Dorrer, H.-D.; Matthies, P. J Appl Polym Sci 1993, 47, 1551.
7. Laun H. M.; Schuch, H. J Rheol 1989, 33(1), 119.
8. Ziabicki, A.; Tian, J. J Non-Newtonian Fluid Mech 1993, 47, 57.
9. Zahorski, S. J Non-Newtonian Fluid Mech 1990, 36, 71.
10. Zahorski, S. J Non-Newtonian Fluid Mech 1993, 50, 65.
11. Zahorski, S. J Non-Newtonian Fluid Mech 1996, 63, 33.
12. Kulkarni, J. A.; Beris, A. N. J Rheol 1998, 42(4), 971.
13. Shimizu, J.; Okui, N.; Kikutani, T. In High-Speed Fiber Spinning; Ziabicki, A.; Kawai, H., Eds.; Wiley-Interscience: New York, 1985.
14. Zieminski, K. F.; Spruiell, J. E. J Appl Polym Sci 1988, 35, 2223.
15. Katayama, K. I.; Yoon, M. G. In High-Speed Fiber Spinning, Ziabicki, A.; Kawai, H., Eds.; Wiley-Interscience: New York, 1985.
16. Patel, R. M.; Bheda, J. H.; Spruiell, J. E. J Appl Polym Sci 1991, 42, 1671.
17. Haward, R. N. J Polym Sci, Polym Phys Ed 1995, 33, 1481.
18. Ward, I. M. Mechanical Properties of Solid polymers, 2nd ed.; Wiley-Interscience: New York, 1983.
19. Treloar, L. R. G. The Physics of Rubber Elasticity, 3rd ed.; Clarendon Press: Oxford, England, 1975.
20. Nakamura, K.; Katayama, K.; Amano, T. J Appl Polym Sci 1973, 17, 1031.
21. Coates, P. D.; Ward, I. M. J Mater Sci 1980, 15, 2897.
22. Nazarenko, S.; Bensason, S.; Hiltner, A.; Baer, E. Polymer 1994, 35, 3883.